The Pb isotope evolution of Bulk Silicate Earth: constraints from its accretion and early differentiation history

Alessandro Maltese[1*] and Klaus Mezger[1,2]

[1]Institute of Geological Sciences, University of Bern, Baltzerstrasse 1+3, 3012 Bern, Switzerland

[2]Center for Space and Habitability, University of Bern, Gesellschaftsstrasse 6, 3012 Bern, Switzerland

(*Corresponding author: Alessandro Maltese alessandro.maltese@geo.unibe.ch)

Key words: Pb isotope evolution, silicate Earth, Earth accretion, Pb paradox

Declarations of interest: none

Abstract

Constraining the evolution of Pb isotopes in the bulk silicate Earth (BSE) is hampered due to the lack of a direct determination of Earth's U/Pb and initial Pb isotope composition. All estimates of these parameters are strongly model dependent and most Pb evolution models start with a meteoritic source, i.e., the primordial Pb composition determined in troilite from the Canyon Diablo iron meteorite. During the condensation of the elements in the solar nebula, accretion of the Earth, and its subsequent chemical evolution, the U/Pb was modified. Different models make different assumptions about the timing and extent of this U-Pb fractionation during Earth's chemical evolution that cannot always be related to known global geological processes at the time of this modification. This study explores geochemical constraints that can be related to known geological processes to derive an internally consistent model for the evolution of the U-Th-Pb systematics of the silicate Earth.

Lead is chalcophile, moderately volatile, and as a result strongly depleted in the BSE compared to primitive meteorites. Any process affecting the abundance and isotope composition of Pb in Earth throughout its early history has to be consistent with the abundance of elements with similar chemical and physical properties in the same reservoir. The abundances of refractory to moderately and highly volatile elements in the BSE imply that the proto Earth was highly depleted in volatile elements and therefore evolved with a very high U/Pb ($^{238}U/^{204}Pb = \mu \geq 100$) prior to collision with the Moon-forming giant impactor. This impactor had close to chondritic abundances of moderately to highly volatile elements and delivered most of Earth's volatile elements, including the Pb budget. Addition of this volatile rich component caused oxidation of Earth's mantle and allowed effective transfer of Pb into the core via sulfide melt segregation. Sequestration of Pb into the core therefore accounts for the high μ_{BSE}, which has affected ca. 53 % of Earth's Pb budget. In

46 order to account for the present-day Pb isotope composition of BSE, the giant impact must
47 have occurred at 69 ±10 Myr after the beginning of the solar system. Using this point in time,
48 a model-derived μ-value, and the corresponding initial Pb isotope composition of BSE, a
49 single stage Pb isotope evolution curve can be derived. The result is a model evolution curve
50 for BSE in ^{208}Pb-^{207}Pb-^{206}Pb-^{204}Pb-isotope space that is fully consistent with geochemical
51 constraints on Earth's accretionary sequence and differentiation history. This Pb-evolution
52 model may act as a reference frame to trace the silicate Earth's differentiation into crust and
53 mantle reservoirs, similar to the CHUR reference line used for other radio-isotope systems. It
54 also highlights the long-standing Th/U paradox of the ancient Earth.
55

Introduction

The U-Pb system is among the most powerful isotope systems for the investigation of Earth's differentiation history. Its application has improved our understanding regarding the age of the Earth (e.g., Gerling, 1942; Holmes, 1946; Houtermans, 1946; Patterson, 1956), the mantle as an evolving and compositionally heterogeneous reservoir (e.g., Gast et al., 1964), as well as the formation and reworking of the continental crust and its recycling back into the mantle (e.g., Tilton & Barreiro, 1980; Zartman & Doe, 1981; Hofmann & White, 1982; Zindler & Hart, 1986; Peucker-Ehrenbrink et al., 1994; Chauvel et al., 1995). At the same time, the compositional spectra of the rocks investigated in these studies have created concerns regarding the fractionation behavior of U and Pb and their timing among the major terrestrial reservoirs. The reason is that the average Pb isotope compositions of these reservoirs, approximated by mid-ocean ridge basalts (MORB – upper mantle), ocean island basalts (OIB – lower mantle), and marine sediments (upper crust) are similar but all of them show an excess in $^{206}Pb/^{204}Pb$ compared to the compositional array of primitive meteorites, the presumed building blocks of the Earth (Fig. 1).

In a Pb evolution diagram showing $^{207}Pb/^{204}Pb$ vs $^{206}Pb/^{204}Pb$, primitive and differentiated meteorites as well as a selection of marine sediments define an isochron, originally termed "Geochron", with an age of 4.55 Ga (e.g., Patterson, 1956). The lowermost point on the Geochron is defined by the primordial Pb isotope composition. It is approximated by the least radiogenic Pb isotope ratios determined on any solar system material, i.e., the Pb isotope composition of troilite from the iron meteorite Canyon Diablo (e.g., Tatsumoto et al., 1973). The fact that all accessible reservoirs on Earth plot to the right of the Geochron, including all estimates for BSE (Fig. 1a), reveals a complexity in the terrestrial U-Pb system that is not seen in other isotope systems. In contrast to the U-Pb

system, isotope systems like Sm-Nd and Lu-Hf that comprise only lithophile refractory elements indicate that the continental crust and the upper mantle are complementary reservoirs. Due to the refractory and lithophile behavior of U and the volatile and chalcophile behavior of Pb, it is problematic to mass balance the Pb isotopes in the bulk silicate Earth (BSE) and use them to trace the evolution and constrain the size of the different silicate reservoirs through Earth's history. This issue of mass balancing the terrestrial Pb isotope evolution has been termed the 1st Pb paradox (e.g., Allègre, 1969). Recent solutions to the problem have searched for a hidden or rarely tapped reservoir that has evolved with a low time integrated U/Pb ($\mu = {}^{238}U/{}^{204}Pb$) to balance the isotopic signatures of the other reservoirs (e.g., Murphy et al., 2003; Hofmann, 2003; Burton et al., 2012). Other efforts have focused on identifying geological mechanisms that affect the element partitioning of U and Pb, such as oxidization and preferential recycling of U into the mantle (e.g., Staudigel et al., 1995), (hydrothermal) transport of Pb into the crust (e.g., Peucker-Ehrenbrink et al., 1994), and retention of Pb in the lower crust or in mantle sulfides (e.g., Hart & Gaetani, 2006). While the sum of these processes is likely to provide an explanation for the similarity in average isotope composition of the different reservoirs, none of these solutions can be used to address the second part of the paradox: the apparent decoupling between the Pb isotope composition of the BSE and the Geochron (Fig. 1). This is because the BSE is a theoretical reservoir that has evolved as a closed system after Earth's accretion was completed and the core had segregated. Afterwards, no geologic process can be applied to this aspect of the paradox. It follows that either the bulk Earth and/or BSE cannot be approximated by a meteoritic composition or that μ_{BSE} changed at least once before closure of the system. In any case, it implies that the "true" Geochron cannot be directly approximated by the meteoritic isochron, but must instead lie to its right and have a shallower slope (e.g., Hofmann et al., 2003). Thus,

104 a review of possible processes that fractionated U-Pb during accretion may help to better
105 understand this issue and identify the processes that caused this aspect of the Pb paradox.
106 This study revisits the effects of Earth's accretion history on the U-Th-Pb isotope
107 systematics and derives a model for the Pb isotope evolution of the BSE. This Pb-evolution
108 model is based on existing literature estimates for the present-day Pb isotope composition for
109 BSE and an accretion and differentiation model for the Earth that is consistent with cosmo-
110 and geochemical constraints for the possible components that make up the Earth as well as
111 the timing of Earth's accretion and internal differentiation. The derived model curves for
112 $^{207}Pb/^{204}Pb$ vs. $^{206}Pb/^{204}Pb$ and $^{208}Pb/^{204}Pb$ vs. $^{206}Pb/^{204}Pb$ can act as reference lines for the Pb
113 isotope evolution of BSE and can potentially be used to further improve our understanding
114 regarding the differentiation history of Earth, as it is done with other radio-isotope systems.

115 **Previous models for the evolution of terrestrial Pb**

116 The Pb isotope composition of the BSE is a parameter that has often been derived in
117 conjunction with solutions to the Pb paradoxes. However, only few studies describe the
118 evolution of terrestrial Pb isotopes in defined reservoirs with concrete model evolution curves
119 in $^{207}Pb/^{204}Pb$ vs. $^{206}Pb/^{204}Pb$ and $^{208}Pb/^{204}Pb$ vs. $^{206}Pb/^{204}Pb$ space. Among those that do, the
120 more prominent models approximate the Pb isotope evolution of the major terrestrial
121 reservoirs by modeling the element cycling between them (e.g., Zartman & Doe, 1981;
122 Zartman & Haines, 1988; Kramers & Tolstikhin, 1997). They produce highly satisfactory
123 solutions to explain the 1st Pb paradox, but do not provide an evolution curve for the BSE.
124 Other studies focused on establishing a single growth curve for the evolution of
125 loosely-defined "terrestrial Pb" (e.g., Doe & Stacey, 1974; Stacey & Kramers, 1975;
126 Cumming & Richards, 1975). Among those, the most widely used model for the discussion
127 of the Pb isotope evolution is that of Stacey & Kramers (1975). Currently, this evolution

128 curve is used routinely for common Pb corrections in U-Pb dating, because it is thought to
129 represent the Pb isotope composition of average crust through time. The initial isotope
130 composition for the model is primordial Pb, as measured in Canyon Diablo troilite. The
131 evolution curve is in part constructed to fit a set of Pb isotope ratios determined on
132 "conformable" or "stratiform" lead ores. These are galena-rich ore deposits that lie parallel to
133 the stratification of enclosing volcano-sedimentary sequences. Their approximate ages are
134 determined relative to absolute ages of other lithologies in the stratigraphic unit. In many
135 such deposits, primary and pristine galena is characterized by homogeneous Pb isotope ratios
136 over a large area of up to tens of kilometers, indicating they are derived from a uniform
137 source (e.g., Stanton and Russell, 1959). The Pb isotope evolution model proposed by Stacey
138 and Kramers (1975) requires a globally significant change in μ and κ ($\kappa = {}^{232}Th/{}^{238}U$) of their
139 source at ~3.7 Ga, in order to accommodate the data from ancient stratiform lead ore deposits
140 and the initial Pb isotope ratios of Canyon Diablo. However, no geological event can be
141 identified that could be associated with the major change of $\mu = 7.19$ before 3.7 Ga to $\mu =$
142 9.74 starting at 3.7 Ga. The same is true for the required concomitant change in κ from 4.6 to
143 3.78. An alternative model for the evolution of "terrestrial Pb" was proposed by Cumming &
144 Richards (1975). Their model uses continuous open system behavior to change μ, implying
145 that core formation, and thus removal of Pb from the silicate reservoir, continued over
146 billions of years; an idea that is inconsistent with stable siderophile-lithophile element ratios
147 in different reservoirs throughout Earth's history (e.g., Newsom et al., 1986; Jochum et al.,
148 1993). While neither of the two studies specifically intended to model the evolution of BSE
149 or the mantle as an analogue, the loose definition of "terrestrial Pb" has often been
150 interpreted to reflect exactly that, which is why other associated caveats are mentioned.

151 In summary, no Pb isotope evolution curve for the BSE has been derived that is fully
152 consistent with the global geological evolution of the Earth. However, the element

153 abundances in BSE and information on the formation and differentiation of the Earth
154 combined with their known timing can be used to develop a model for the Pb evolution of
155 BSE that fits all known events and processes that could have affected the U-Pb system
156 globally.

157 # Methods

158 ## The accretion of the Earth

159 The composition of the Earth and its accretion history are questions that have long
160 been investigated using element abundances and isotope compositions of meteorites, which
161 are considered its possible building blocks (e.g., Ganapathy & Anders, 1974; Anders, 1977;
162 Morgan & Anders, 1980; Wänke, 1981; Sun, 1982). In view of these criteria it has been
163 shown that the Earth likely has an end member composition with respect to meteorites (e.g.,
164 Burkhardt et al., 2011; Render et al., 2017) and cannot be formed by accretion or mixing of
165 only currently known materials in the solar system. This suggests that the accretion and
166 differentiation of the Earth is the result of a unique sequence in terms of early solar system
167 processes and their relative timing, which have formed Earth with its present composition. A
168 key element of many models is that the Earth formed from various amounts of chemically
169 very distinct materials. The relative composition of the refractory and volatile elements of the
170 Earth as well as the depletion of Earth's mantle in redox-sensitive siderophile elements can
171 be explained by a two-component mixture (e.g., Wänke & Dreibus 1988; O'Neill, 1991;
172 Albarède et al., 2009; Rubie et al., 2015; Ballhaus et al., 2017): 1) a major component that
173 was highly volatile element depleted and reduced, with 2) a minor component that was
174 relatively volatile rich and oxidized. Together, the two components make up at least 99 % of
175 the solid Earth. Some evidence for this pathway can be extracted from the relative element

abundances in the BSE, as they represent the final product of the entire accretion history (Fig. 2; e.g., Wänke & Dreibus, 1988; O'Neill, 1991).

The highly refractory lithophile and moderately volatile lithophile elements define a step function in BSE, each with relative CI abundance, but with a ca. 6 to 7-fold difference (Fig. 2, Lodders, 2003; Wang et al., 2018). This step may define the (relative) contribution and initial composition of the two components that make up the Earth. These observations are consistent with the model of Wänke & Dreibus (1988) regarding the differences in size and compositions of Earth's two major building blocks. Thus, proto-Earth might have accreted almost free of volatile elements and subsequently mixed with a volatile undepleted body (e.g., Albarède et al., 2009; Ballhaus et al., 2017). The siderophile elements are strongly depleted in BSE, which is commonly attributed to core formation by segregation of an Fe-melt from the silicate mantle. Likewise, almost all chalcophile elements such as Cd, Tl, and Pb are also strongly depleted. Assuming these chalcophile and moderately volatile elements were delivered by the minor component, their low abundance is in part the result of the size difference between the two bodies that made up the Earth (Fig. 2). An additional depletion of chalcophile elements after addition of the second component to the Earth was likely caused by segregation of a sulfide melt during the final stages of core formation (e.g., O'Neill, 1991). Based on these observations, Pb depletion in the BSE relative to the solar system abundance of the elements is due to two very distinct processes: 1) the initial extreme depletion of Earth in volatile elements due to incomplete condensation of volatile elements from the solar nebula and 2) removal of Pb from the mantle via a sulfide melt after mixing of the volatile element depleted proto-Earth with a smaller oxidized component.

198 **Earth's accretion from a U-Pb perspective**

199 In order to integrate the Pb isotope evolution in BSE with the accretion and
200 differentiation of the Earth, the following assumptions are made regarding the two mixing
201 components: The abundances of lithophile elements in BSE can be reproduced by mixing of
202 85 % of material that is highly volatile depleted and reduced (i.e., proto-Earth) and 15 % of
203 material that is undepleted in volatile elements and oxidized. The proportions are derived
204 from the abundance of the lithophile refractory and moderately volatile elements in BSE,
205 which are not affected by core formation processes (Fig. 2, S-Table 1; e.g., O'Neill, 1991).
206 They are consistent with the sizes of the two bodies inferred from models that argue for the
207 formation of the Moon by a giant-impact (e.g., Benz et al., 1989; Canup & Asphaug, 2001),
208 and are therefore treated to correspond to the same event. These constraints obtained from the
209 lithophile elements have implications for the Pb isotope evolution in BSE following accretion
210 and differentiation of the Earth. Both components formed from the solar nebula within the
211 very first million years of the solar system, and thus initially had primordial Pb isotope
212 compositions, albeit different volatile element abundances, and thus different U-Pb ratios.
213 The proto-Earth accreted from highly volatile element depleted material, with a high
214 $^{238}U/^{204}Pb$ ($\mu \geq 100$), while a CI chondritic composition is assumed for Theia, the giant
215 impactor (ca. $\mu = 0.19$, Allègre et al., 1995). Due to the refractory character of both U and
216 Th, both bodies accreted and evolved with a κ equal to primordial composition ($\kappa = 3.88$,
217 Blichert-Toft et al., 2010). Each body evolved independently until their collision and
218 subsequent complete mixing, in fractions of 0.85 and 0.15, yielding the initial Pb isotope
219 composition of the BSE. Model parameters and constants are summarized in Table 1. All
220 errors are propagated from the initial uncertainties of their individual contribution (S-

221 Table 1). The following equations describe the isotope compositions and evolution of each
222 body at time t_2:

223 $$\left(\frac{^{206}Pb}{^{204}Pb}\right)_{t2} = \left(\frac{^{206}Pb}{^{204}Pb}\right)_{t1} + \mu\left(e^{\lambda_x t1} - e^{\lambda_x t2}\right)$$

224 $$\left(\frac{^{207}Pb}{^{204}Pb}\right)_{t2} = \left(\frac{^{207}Pb}{^{204}Pb}\right)_{t1} + \left(\frac{\mu}{137.82}\right)\left(e^{\lambda_y t1} - e^{\lambda_y t2}\right)$$

225 $$\left(\frac{^{208}Pb}{^{204}Pb}\right)_{t2} = \left(\frac{^{208}Pb}{^{204}Pb}\right)_{t1} + \omega\left(e^{\lambda_z t1} - e^{\lambda_z t2}\right)$$

226 with $\omega = {}^{232}Th/{}^{204}Pb$, the present-day best-estimate ${}^{238}U/{}^{235}U = 137.82$ (Hiess et al., 2012),
227 $\lambda_{x,y,z}$ the decay constants of ^{238}U, ^{235}U, ^{232}Th (Jaffey et al., 1971, Le Roux & Glendenin,
228 1963), and the beginning of the solar system t_1, with Canyon Diablo primordial Pb isotope
229 composition.

230 Figure 3 illustrates the model in Pb isotope space for a t_2 = 60 to 160 Myr after the
231 start of the solar system. Due to its high μ-value, the proto-Earth evolved rapidly to highly
232 radiogenic Pb isotope ratios (Fig. 3a). In contrast, the Pb isotopes in Theia did not evolve
233 much beyond the primordial Pb isotope composition during the first 160 Myr of the solar
234 system (Fig. 3b and d). The two components were mixed during or shortly after the giant
235 impact. Each possible initial Pb isotopic composition of the BSE (BSE_{ini}) is a function of the
236 relative contributions of the two bodies and the time of mixing. Its composition lies closer to
237 the minor, i.e., undeleted component, because of the very low elemental abundance of Pb in
238 the proto-Earth. Anywhere from the mixing array (BSE_{ini}), an evolution curve for the BSE
239 can be constructed resulting in a present-day Pb isotope composition that plots to the right of
240 the meteorite isochron (the apparent Geochron) and in the range of the different published
241 estimates for BSE (Fig. 3a and c). Using estimates of the BSE Pb isotope compositions from
242 the literature as target values, the timing of the mixing event can be deduced. By varying μ_{BSE}

243 for every possible time of collision and mixing as starting point, the decay equation is solved
244 to yield the best fit between model and literature data, and thus the initial Pb isotope
245 composition of BSE and the time of the giant impact are constrained.

246 ## Results

247 Figure 4 shows a plot of literature estimates and corresponding model results for BSE
248 in Pb isotope space. The model successfully reproduces the BSE estimates of all chosen
249 studies. The numbers correspond to the mixing time of the two major components that make
250 up the BSE in the proportion 85:15, in Myr after the beginning of the solar system. The
251 estimates for BSE have very similar $^{207}Pb/^{204}Pb$ and differ mostly in terms of $^{206}Pb/^{204}Pb$ and
252 $^{208}Pb/^{204}Pb$, which lead to later mixing times the higher both of these ratios are. In contrast,
253 higher $^{207}Pb/^{204}Pb$ ratios lead to earlier mixing times due to the shorter half-life of ^{235}U and
254 the resulting rapid ingrowth of ^{207}Pb during the early history of the solar system. In Fig. 4a, a
255 sharp increase in mixing times can be seen between the estimates of Galer & Goldstein
256 (1991) and Kamber & Collerson (1999), which again is mainly a function of increasing
257 $^{206}Pb/^{204}Pb$. The estimate of Kramers & Tolstikhin (1997) is likely an outlier because the BSE
258 composition was not purposefully constrained in their model calculations (Murphy et al.,
259 2003). Based on the calculated timing of mixing, the estimates for the Pb isotope composition
260 of BSE can be combined into two groups, with average times for the mixing event of
261 69 ±10 Myr and 125 ±34 Myr after the beginning of the solar system (Table 2). Each BSE
262 estimate can only be reproduced at one specific point in time, within a tight age range of ~2-
263 3 Myr for which μ will vary slightly (< 0.1 % difference). Solutions with young ages require
264 μ-values between ca. 8.4 and 8.7 (8.6 on average) while the other grouping requires μ-values
265 between ca. 8.9 and 9.5 (9.1 on average). In the $^{208}Pb/^{204}Pb$ vs. $^{206}Pb/^{204}Pb$ diagram (Fig. 4b),
266 the mixing times increase diagonally towards more radiogenic values. The same grouping is

observed, except with no correlation between the required κ and mixing time; the average κ is 4.1.

The different ages obtained for the formation of BSE can, to some extent, be explained by the assumptions invoked by the different models. Davies (1984) deliberately chose an isotopic composition for the BSE that plots close to the meteoritic isochron. Similarly, Galer & Goldstein (1991), who used the approach of Allègre & Liew (1989), forced the BSE values to lie close to the apparent Geochron. The estimate of Kwon et al. (1989) is based on isotope compositions of magmatic alkaline complexes as target values. Finally, Allègre et al. (1988) and Allègre & Liew (1989) used the mean isotope composition of Ocean Island Basalts (OIBs) as target values. In the remaining studies BSE was not forced to lie within a predetermined range. Most models account for the effects of accretion and core formation, often by assuming an initial low-μ stage and restarting the Pb isotope evolution with Canyon Diablo isotope composition or slightly more evolved values between 4.52 and 4.50 Ga, after core formation was completed (e.g., Liew et al., 1991; Kwon et al., 1989). Generally, the studies for which earlier mixing times are obtained assume that core formation progressed relatively fast or in a single catastrophic event within the first ca. 65 Myr of Earth's accretion (e.g., Galer & Goldstein, 1996; Murphy et al., 2003). Those for which ages indicating later U-Pb fractionation are obtained assume that core formation progressed more slowly, lasting 100 Myr or longer, and hence start their U-Pb evolution model only around 4.45 Ga (e.g., Zartman and Haines, 1988).

Discussion

The isotope composition of the BSE is commonly used as a reference reservoir for the evaluation of differentiation processes throughout Earth's history. However, μ_{BSE} and its initial isotope composition are poorly constrained because multiple changes of the parent-

daughter ratios are required throughout Earth's history. This is problematic because except for the primordial Pb isotope composition, no other parameter can be measured directly or deduced from analyses of primitive meteorites or their components, as it is possible with isotope systems like Sm-Nd or Lu-Hf. The latter include only refractory and lithophile elements which are neither affected by volatile element loss during the accretion process nor by core formation during the early stages of Earth's evolution. Thus, planetesimals and planets preserve chondritic relative abundances of these systems (e.g., Bouvier et al., 2008; Burkhardt et al., 2011; Iizuka et al., 2015). Using literature estimates for BSE, a range of scenarios concerning possible compositions and the timing of these changes in U-Pb ratios can be derived (Fig. 4). A comparison of the model results and their underlying assumptions with independent constraints regarding these early geological processes and events allows identification of the most consistent scenarios. If these are then applied to the U-Pb systematics, it is possible to derive the isotope evolution of a model BSE within a solid framework that considers geological mechanisms for U-Pb fractionation as well as timing.

The Earth-Moon system

Literature estimates for the Pb isotope composition of BSE are used as input parameters in an evolution model in order to determine the initial Pb isotope composition of the BSE based on mixing of the proto-Earth with the giant impactor Theia, in proportions constrained by the relative abundances of lithophile elements in BSE (0.85:0.15, Fig. 2). Consequently, the time at which the two components mixed and the resulting initial Pb isotope composition of the BSE is established, also constrains the timing of the formation of the Moon. The latter has long been a focal point of attention of cosmochemical research and a complete discussion is beyond the scope of this paper. However, a number of constraints exist with which the Pb isotope evolution model has to be consistent with: The oldest mineral

315 dated from the Moon is a zircon with a U-Pb age of 4.417 ±6 Ma, providing an absolute
316 minimum age for the formation of the Moon (Nemchin et al., 2009). All distinct lunar mantle
317 reservoirs, i.e., KREEP, mare basalts, Mg-suite norite, and the Kalahari lunar meteorite have
318 identical $^{182}W/^{184}W$ isotope signatures despite having different Hf/W (e.g., Touboul et al.,
319 2015; Kruijer et al., 2015). In addition, the weighted mean of these reservoirs shows a well-
320 resolved ^{182}W excess of 26 ±3 ppm compared to the BSE (Kruijer and Kleine, 2017). These
321 characteristics have been used to put constraints on the earliest time of lunar differentiation.
322 These vary, depending on the assumptions, between 40-60 Myr (Thiemens et al., 2019) and
323 >70 Myr after solar system formation (Kruijer and Kleine, 2017). In addition, an average Lu-
324 Hf model age of ca. 60 ±10 Myr (1σ) was calculated using the four least-radiogenic initial Hf
325 isotopic compositions obtained from KREEP-zircon (Barboni et al., 2017). Recalculating this
326 age by weighing the individual data points according to their assigned errors and applying a
327 student's-t multiplier results in an age of 62 ±24 Myr (95 % conf.). Lastly, a Rb-Sr model age
328 of 87 ±13 Myr was obtained by calculating the $^{87}Sr/^{86}Sr$ lunar initial (LUNI; Carlson and
329 Lugmair, 1988) from CAI or angrite isotope compositions and Rb/Sr = 0.03 (Halliday, 2008).
330 While none of these estimates is free of assumptions, they also carry a lot of weight in that
331 they are built around well-determined and robust isotopic constraints. The good agreement
332 between different independent isotope systematics suggests that the Moon formed early, i.e.,
333 within the first 100 Myr of the solar system.

334 Samarium-Nd, Rb-Sr, Lu-Hf, as well as Pb-Pb isotopic measurements define
335 isochrons and model ages for lunar rocks between 4.34 and 4.37 Ga or ca. 200-230 Myr after
336 beginning of the solar system (e.g., Carlson et al., 2014; Snape et al., 2016; Borg et al., 2011,
337 2015, 2019). The lithologies investigated in these studies cover a large area and sample both
338 crustal and mantle reservoirs, indicating they record primordial differentiation during
339 crystallization of the lunar magma ocean. This interpretation, albeit the easiest of the results,

340 is inconsistent with the "old" Hf and Sr lunar model ages, the oldest terrestrial model ages
341 from Archean rocks (e.g., Kemp et al., 2010; Morino et al., 2017), and younger than the
342 oldest zircon on the Moon (Nemchin et al., 2009). While the two discussed age ranges for the
343 Moon are both built around robust isotopic data, they cannot be tracing the same geologic
344 event. This controversy remains a vivid topic of discussion within the field of
345 cosmochemistry.

346 Based on these estimates, BSE Pb isotope estimates from the younger grouping (wtd.
347 avg. 2, Table 2) do not yield results consistent with the timing of Moon formation. The
348 remaining estimates define a relatively tight corridor for possible Pb isotope signatures of the
349 BSE. From this cluster, an average mixing time of 69 ±10 Myr after the beginning of the
350 solar system is obtained (wtd. avg. 1, Table 2). This is in broad agreement with constraints
351 from Hf-W, Lu-Hf, and Rb-Sr isotope systematics. Using the composition of the Nantan iron
352 meteorite (Blichert-Toft et al., 2010) the obtained mixing time would be younger by ca.
353 5 Myr. Here, the composition of Canyon Diablo is preferred because the model starts at the
354 beginning of the solar system and therefore using the more primitive Pb isotopic composition
355 is appropriate.

356 **The effect of core formation on the U-Pb systematics of the BSE**

357 The difficulty in determining the Pb isotope composition of the BSE stems in part
358 from the observation that Pb has to partition to some extent into the core during Earth's
359 accretion (e.g., Oversby & Ringwood, 1971). It was proposed early that this process is likely
360 the cause of the high μ-value of the mantle and BSE (μ = 7-10) that contrasts with the low μ-
361 value observed in chondritic meteorites (μ <1, Allègre et al., 1995). The degree of this so-
362 called "core-pumping" and the timescale, over which it occurred, have drastic effects on μ_{BSE}
363 and its time integrated Pb isotope composition. Likewise, the timing and magnitude of this

process needs to be reconciled with the (relative) abundances and distribution of other elements, especially the siderophile and chalcophile elements in the BSE (Fig. 2). An important parameter that controls the chemical affinities of these elements is the oxygen fugacity (fO_2) of the mantle. This parameter also influences the possible formation of Fe-melts. Under reducing conditions, Fe occurs as metal and segregates into the core together with other siderophile elements. Oxidizing conditions promote the segregation of a sulfide melt in the magma ocean, as Fe becomes ferrous (lithophile). Extraction of such a sulfide melt promotes the depletion of chalcophile elements in the co-existing silicate melt (e.g., O'Neill, 1991).

Different accretion models for the Earth have been proposed that take these possible processes into consideration (Wänke & Dreibus, 1988; O'Neill, 1991; Albarède et al., 2009; Rubie et al., 2015; Ballhaus et al., 2017). In these models it is suggested that Earth originates initially from reduced and volatile element depleted material and that volatile-rich material was accreted during a later stage. On this basis, it follows that the proto-mantle was initially reduced and became oxidized later through addition of the volatile-rich material and homogenization in a global magma ocean (e.g., Wade & Wood, 2005; Wood et al., 2006). With increasing fO_2, the solubility of S in silicate melts decreases strongly (e.g., Holzheid & Grove, 2002; Moretti & Ottonello, 2005). Therefore, core formation can be sharply divided into two distinct stages: 1) The segregation of an Fe-rich metallic melt (reduced mantle) followed by 2) segregation of sulfide melt (oxidized mantle). Experimental studies have shown that Pb is primarily chalcophile (e.g., Jones & Drake, 1986; Jones et al., 1993). Consequently, the depletion of Pb and other siderophile/chalcophile and volatile elements in the BSE can be attributed to the segregation of a sulfide melt, the "Hadean matte" (e.g., O'Neill, 1991; Wood & Halliday, 2005; Lee et al., 2007; Kiseeva & Wood, 2015; Laurenz et al., 2016), in a single event right after the giant impact. The proposed pronounced change in

389 fO_2 is consistent with the observation that the siderophile elements Fe and Ga occur in
390 relative chondritic abundances similar to the strongly lithophile moderately volatile elements
391 in BSE, which are inherited from Theia (Fig. 2, component B). This is because both Fe and
392 Ga are lithophile under oxidizing conditions (Righter, 2011) which further implies that, as the
393 two components mixed, core formation continued via segregation of sulfide melts.

394 The consequence of this accretionary sequence was that mixing of proto-Earth with
395 Theia lowered μ_{BSE} to ca. 3.54 and subsequent sulfide segregation caused an instantaneous
396 increase of μ_{BSE} shortly after the giant impact. Thus, by comparing the initial concentration of
397 ^{204}Pb in BSE obtained from the mixing model to the estimated ^{204}Pb abundances of the
398 primitive mantle (Galer & Goldstein, 1996), it is possible to calculate a depletion factor of Pb
399 for the BSE. The CI-normalized concentrations of ^{204}Pb in BSE_{ini} (this study) and the
400 primitive mantle are 0.053 and 0.025 respectively. By this comparison, about 53 % of Pb was
401 removed during the second stage of core formation, assuming that Theia delivered Pb in CI
402 chondritic abundance relative to the refractory elements. This is a maximum estimate as it
403 does not account for Pb lost from the Earth's mantle by volatilization during the giant impact
404 and escape from the Earth's Roche limit (e.g., Connelly & Bizzarro, 2016).

405 Another consequence of these geochemical relationships is that the idea of an initial
406 low-μ stage for proto-Earth, is inconsistent with core formation by metal-silicate segregation.
407 Since U is refractory and lithophile, it was delivered in CI chondritic abundances. A low-μ
408 therefore implies that the same is true for Pb, meaning the proto-Earth had a CI bulk
409 chondritic composition. Thus, the volatility budget, and therefore fO_2 of the mantle would
410 have been too high during accretion, Fe would have been ferrous, such that siderophile and
411 chalcophile metals could not have segregated except by sulfide segregation. Further, it would
412 be arbitrary to assume the presence of Pb without the presence of other volatile elements, and
413 thus to a certain degree, the presence of water in the form of OH^-, which ultimately leads to

414 the same problem. Consequently, the most coherent solution is to assume that the proto-Earth
415 was essentially volatile free, which also significantly increases the likelihood that the giant
416 impactor provided a major part of the Earth's volatile budget as well as water; in view that
417 the late veneer can only account for ca. 0.5 % of material of the BSE (e.g., Becker et al.,
418 2006).

419 **The Pb-isotope composition of the BSE**

420 The isotopic composition of the BSE acts as a reference reservoir in many
421 geochemical studies that discuss the differentiation of the Earth. In detail, the Pb isotope
422 composition of BSE can be modelled using the primordial composition of Canyon Diablo as
423 a starting value in combination with a model for the chemical composition of the different
424 components that make up the Earth (Fig. 2). Then, by comparing the canonical mixing times
425 with those obtained from estimates for the Pb isotope composition of present-day BSE
426 (Fig. 4), an internally consistent model for the Pb evolution in BSE is derived. The average of
427 solutions, in agreement with independent geological and geochemical constraints, yields an
428 initial Pb isotope composition of the BSE of $^{206}Pb/^{204}Pb = 9.345$, $^{207}Pb/^{204}Pb = 10.37$, and
429 $^{208}Pb/^{204}Pb = 29.51$, with $\mu_{BSE} = 8.63 \pm 0.06$ and $\kappa_{BSE} = 4.05 \pm 0.20$ (Table 2). The latter value
430 is indistinguishable from independent estimates of the solar system value of $\kappa_{ssytem} =$
431 3.876 ± 0.016 and $\kappa_{BSE} = 3.90 \pm 0.13$ (Blichert-Toft et al., 2010; Wipperfurth et al., 2018). The
432 increase in μ_{BSE} occurred ca. 69 Myr after the birth of the solar system, which also
433 corresponds to the time of the Moon-forming giant impact. The derived parameters can be
434 used to construct a BSE isotope evolution curve for the U-Th-Pb systematics, with a present-
435 day composition of $^{206}Pb/^{204}Pb = 18.05$, $^{207}Pb/^{204}Pb = 15.56$, and $^{208}Pb/^{204}Pb = 38.2$ (Fig. 5
436 and S-Table 2):
437

438 $$\left(\frac{^{206}Pb}{^{204}Pb}\right)_{t2} = 9.345 + 8.63\left(e^{\lambda_x 4.5Ga} - e^{\lambda_x t2}\right)$$

439 $$\left(\frac{^{207}Pb}{^{204}Pb}\right)_{t2} = 10.37 + \left(\frac{8.63}{137.82}\right)\left(e^{\lambda_y 4.5Ga} - e^{\lambda_y t2}\right)$$

440 $$\left(\frac{^{208}Pb}{^{204}Pb}\right)_{t2} = 29.51 + 34.8\left(e^{\lambda_z 4.5Ga} - e^{\lambda_z t2}\right)$$

441

442 with $\lambda_{x,y,z}$ the decay constants of ^{238}U, ^{235}U, and ^{232}Th (Jaffey et al., 1971, Le Roux &
443 Glendenin, 1963) and t_1 = 4.498 Ga.

444 The trajectory of the Pb evolution curves is strikingly similar to the isotopic
445 compositions of Pb ores, i.e., galena from stratiform deposits. This is unexpected because of
446 the ambiguity related to the origin of these minerals. Originally, the homogeneity and time-
447 integrated alignment of these ores was interpreted to reflect derivation from a reservoir that is
448 larger and more homogeneous than the continental crust, i.e., the mantle (e.g., Russell, 1956;
449 Wilson, 1956). A crustal origin was later suggested, in part because the Pb isotope ratios of
450 young, unaltered volcanic rocks can differ significantly (up to >10 %) among the volcanic
451 suites, but also from the galena growth curve, which argues against a uniform deep-seated
452 source for Pb ores. A detailed discussion on this matter can be found in Richards (1971), who
453 advised episodic or continuous models to be used, but also concluded that model ages of ores
454 have no exact geological significance. It has also been pointed out that in recent metalliferous
455 sediments the Pb isotopic compositions are quite heterogeneous, and thus cannot represent a
456 homogenous mantle source but show the influence of different high-μ crustal contributions
457 (Peucker-Ehrenbrink et al., 1994). Lastly, the youngest Pb ores have isotopic compositions
458 indistinguishable from average river and oceanic sediments, again indicating they are derived
459 from crustal sources (Hofmann, 2001). Overall, it can be argued that Pb ores in stratiform

460 deposits constitute a mix of mantle and crustal material that depends on the composition of
461 the volcano-sedimentary unit they are derived from, the nature of the process by which these
462 ores formed, and the time passed between magmatic emplacement and ore formation.

463 However, for the Archean the differences in Pb isotope compositions between
464 continental crust and mantle are much smaller than for the present-day situations due to the
465 dominance of juvenile crust in the Archean. Thus, if the time interval between mantle
466 melting, emplacement, and ore formation was relatively short, ancient Pb ores might indeed
467 approximate the isotopic composition of the isochronous mantle. Support for this hypothesis
468 potentially lies in the good match observed in $^{207}Pb/^{204}Pb$ vs $^{206}Pb/^{204}Pb$ isotope space
469 (Fig. 5a). The fit, as approximated by the time-integrated model composition relative to that
470 of galena, is better than 1 % at any time before 3 Ga (Table 3). In addition, uranogenic Pb
471 model ages calculated against our proposed BSE initial Pb isotopic composition agree within
472 1.4 % or better. This concordance not only indicates that ancient Pb ores could be
473 representative of the mantle, but also that the nature of this mantle source was primitive.

474 A comparison of the galena data with the new model curves for BSE reveals a better
475 fit in $^{208}Pb/^{204}Pb$ vs $^{206}Pb/^{204}Pb$ space, for galena younger than ~3 Ga compared to older
476 samples. If an isotope evolution curve is purposefully fit to the Pb isotope composition of
477 ancient galena, using BSE_{ini} (Fig. 5, black curves), the average agreement between model
478 curve and the isotope ratios of the ancient galena improves significantly (<0.20 % scatter),
479 but induces significant changes in parent-daughter ratios (μ_{galena} = 8.42 and κ_{galena} = 4.27).
480 Subsequently, the isotope evolution curves deviate from younger galena. This 'kink' is best
481 observed in $^{208}Pb/^{204}Pb$ vs $^{206}Pb/^{204}Pb$ isotope space where an apparent transition towards a
482 lower κ-value can be seen between ca. 3 and 2 Ga (Fig. 5b); which also implies a
483 concomitant increase in μ-value during the same time frame. It has been shown
484 experimentally that U is more chalcophile than Th under reducing conditions and could have

485 partitioned into the core during sulfide segregation, thereby instantly increasing κ_{mantle} and
486 decreasing μ_{mantle} (Wohlers & Wood, 2017). Later re-equilibration at the core-mantle
487 boundary then let to the observed gradual reverse. An indication of this process are estimates
488 of $\kappa_{modern\ mantle}$ and κ_{crust} of 3.87 and 3.95 respectively, which yield a mass weighted estimate
489 for BSE of 3.90 (Wipperfurth et al., 2018). However, the same authors have shown by Monte
490 Carlo simulation that core formation has only a negligible effect on κ_{BSE}. In addition, sulfide
491 melt segregation requires oxidizing conditions to occur and to date, the chemical affinities of
492 U and Th in oxidized, sulfur-bearing environments are not well understood.

493 Thus, the instantaneous change from the proposed μ_{BSE} and κ_{BSE} to the galena values
494 might instead have occurred after accretion was completed, followed by a progressive change
495 during the late Archean. An alternative process that could change κ is fractional
496 crystallization of Mg-silicate perovskite (MgPv) during magma ocean crystallization. Under
497 high P/T conditions (ca. 26 GPa and >2000 °C), the partition coefficient of U into perovskite
498 is up to four times higher than Th allowing for effective element fractionation (e.g., Liebske
499 et al., 2005). Such a fractionation could have imparted a low κ on the deeper parts of the
500 mantle and a higher κ on the shallower parts, attributed to changes in the U concentration in
501 the upper mantle. Deep mantle convection slowly erased this stratification so that the Pb
502 isotope composition of ancient (>3 Ga) galena requires a lower μ and higher κ compared to
503 those that formed after ca. 2.75 Ga ('kink' in Fig. 5b). However, the partition coefficients of
504 U into MgPv are only as high as $D_U = 0.2$ meaning that substantial fractionation is required to
505 raise the Th/U of the residual liquid significantly. Another problem is that Pb is much more
506 compatible in MgPv (up to $D_{Pb} = 1.46$) and would thus lead to an increase of U/Pb in the
507 residual melt rather than a decrease, as predicted by the ancient galena. This mechanism
508 therefore additionally requires that MgPv crystallization occurred during or shortly after the
509 sulfide segregation which effectively removed Pb from the silicate melt.

A full discussion of this issue is far beyond the scope of this paper, but it appears that the current solutions to this paradox remain speculative. Despite this, the proposed Pb model not only highlights the existence of this paradox, but also allows its quantification which can eventually be tested against new solutions of this issue.

Conclusions

The element abundances and isotope compositions of the refractory lithophile elements in Earth are very similar to primitive meteorites. However, the observed μ of the BSE is much higher and its Pb isotope composition more radiogenic than in any of Earth's potential parent bodies. These differences require fractionation of U from Pb during Earth's accretion or shortly thereafter. Previously, these processes were attributed to global differentiation events, for which however no geologic evidence exists (e.g., Stacey & Kramers, 1975). Some models require core formation to continue throughout Earth's history, which were later rebutted (c.f., Cumming & Richards, 1975; Newsom et al., 1986; Jochum et al., 1993). In other cases, and due to the lack of direct geochemical constraints, many models use an initial BSE Pb isotope composition equal to primordial Pb (e.g., Zartman & Haines, 1988) and assume a closure age of 4.45 Ga for BSE to account for the effects of core formation (e.g., Doe & Stacey, 1974). For this study, literature estimates for the Pb isotope composition of BSE have been examined and brought in agreement with a planetary accretion model for the Earth. The model requires only a minimum of assumptions, i.e., a volatile depleted proto Earth (with a high μ-value) and the delivery of the majority of volatile elements by the giant impactor. Support for these model constraints are found in the element and isotope abundances observed in the BSE (e.g., Wänke & Dreibus, 1988; Albarède et al., 2009; Rubie et al., 2015; Ballhaus et al., 2017). Using these constraints, an internally consistent model is derived that broadly reproduces the potential time of the giant impact, the

534 elevated μ-value of the BSE, and the initial and present-day Pb isotope composition of the
535 undifferentiated mantle, thus removing the first Pb paradox. This model for the Pb isotope
536 evolution of the BSE is fully consistent with geochemical constraints and the accretion
537 history of the Earth, particularly the volatile budget, the final major accretion by a giant
538 impact, and core formation.

539 The Pb paradox of the BSE can be understood in terms of a heterogeneous
540 distribution of volatile elements in the two main components that made up the Earth. The
541 existence of two components with very distinct volatile element budget implies that they
542 likely accreted in different parts of the solar system. Therefore, it is possible that the
543 establishment of the Pb isotope systematics in the primitive mantle is the result of the same,
544 single catastrophic chance event that also formed the Moon and brought the volatiles to
545 Earth. This event is the giant impact which occurred 69 ±10 Myr after the beginning of the
546 solar system; in agreement with estimates for the crystallization of the lunar magma ocean.
547 The collision caused large scale melting of the mantle and the second stage of core formation
548 in the form of segregation of sulfide melts, by which ca. 53 % of Earth's Pb budget was
549 removed from the mantle generating the present high μ-value observed in the silicate
550 reservoir of the Earth. The resulting Pb isotope evolution curves ($^{207}Pb/^{204}Pb$ vs $^{206}Pb/^{204}Pb$
551 and $^{208}Pb/^{204}Pb$ vs $^{206}Pb/^{204}Pb$, Fig. 5) allow for a more robust discussion of Earth's
552 differentiation history because they are closely tied to a geological context and do not require
553 any assumptions regarding the Pb isotope composition or evolution of any of the major
554 terrestrial reservoirs. It can serve as a reference frame to understand the chemical
555 differentiation of the silicate Earth into different reservoirs over time, similar to the CHUR
556 reference for the Lu-Hf and Sm-Nd isotope systems that can be used for mass-balancing
557 crustal growth and concomitant mantle depletion (e.g., Doe & Zartman, 1979; Kramers &

Tolstikhin, 1997). Finally, it provides a tangible frame for the Th/U paradox of the ancient mantle and might prove to be potentially useful for its solution.

Acknowledgements

This study was supported through SNF grant 17452. Additional support was provided by NCCR PlanetS supported by the Swiss National Science Foundation grant nr. 51NF40-141881. We would like to thank A.W. Hofmann for an extensive and critical review as well as two anonymous reviewers who helped improve the quality of the manuscript. We also like to thank Yuri Amelin for additional comments and editorial efforts, and Jeffrey G. Catalano as Executive Editor.

Research data

The complete data set can be downloaded from the associated Mendeley Data Repository: http://dx.doi.org/10.17632/r63n3b9rm8.2

References

Albarède, F., 2009. Volatile accretion history of the terrestrial planets and dynamic implications. *Nature* **461**, 1227–1233. https://doi.org/10.1038/nature08477

Allègre, C.J., 1968. Comportement des systèmes U-Th-Pb dans le manteau supérieur et modèle d'évolution de ce dernier au cours des temps géologiques. *Earth Planet. Sci. Lett.* **5**, 261–269. https://doi.org/10.1016/S0012-821X(68)80050-0

Allègre, C.J., Lewin, E., 1989. Chemical structure and history of the Earth: evidence from global non-linear inversion of isotopic data in a three-box model. *Earth Planet. Sci. Lett.* **96**, 61–88. https://doi.org/10.1016/0012-821X(89)90124-6

Allègre, C.J., Lewin, E., Dupré, B., 1988. A coherent crust-mantle model for the uranium-thorium-lead isotopic system. *Chem. Geol.* **70**, 211–234. https://doi.org/10.1016/0009-2541(88)90094-0

Allègre, C.J., Manhès, G., Göpel, C., 1995. The age of the Earth. *Geochim. Cosmochim. Acta* **59**, 1445–1456. https://doi.org/10.1016/0016-7037(95)00054-4

Anders, E., 1977. Chemical compositions of the Moon, Earth, and eucrite parent body. *Philos. Trans. R. Soc. London. Ser. A, Math. Phys. Sci.* **285**, 23–40.

https://doi.org/10.1098/rsta.1977.0040

Azbel, I.Y., Tolstikhin, I.N., Kramers, D., Pechernikova, V., Vityazev, A. V., 1993. Core growth and siderophile element depletion of the mantle during homogeneous Earth accretion. *Geochim. Cosmochim. Acta* **57**, 2889–2898. https://doi.org/10.1016/0016-7037(93)90396-E

Baadsgaard, H., Nutman, A.P., Bridgwater, D., Rosing, M., McGregor, V.R., Allaart, J.H., 1984. The zircon geochronology of the Akilia association and Isua supracrustal belt, West Greenland. *Earth Planet. Sci. Lett.* **68**, 221–228. https://doi.org/10.1016/0012-821X(84)90154-7

Ballhaus, C., Fonseca, R.O.C., Münker, C., Rohrbach, A., Nagel, T., Speelmanns, I.M., Helmy, H.M., Zirner, A., Vogel, A.K., Heuser, A., 2017. The great sulfur depletion of Earth's mantle is not a signature of mantle–core equilibration. *Contrib. to Mineral. Petrol.* **172**, 1–10. https://doi.org/10.1007/s00410-017-1388-3

Barboni, M., Boehnke, P., Keller, C.B., Kohl, I.E., Schoene, B., Young, E.D., Mckeegan, K.D., 2017. Early formation of the Moon 4.51 billion years ago. *Sci. Adv.* **3**, e1602365. https://doi.org/10.1126/sciadv.1602365

Benz, W., Cameron, A.G.W., Melosh, H.J., 1989. The origin of the Moon and the single impact hypothesis III. *Icarus* **81**, 113–131. https://doi.org/10.1006/icar.1996.5642

Blichert-Toft, J., Zanda, B., Ebel, D.S., Albarède, F., 2010. The Solar System primordial lead. *Earth Planet. Sci. Lett.* **300**, 152–163. https://doi.org/10.1016/j.epsl.2010.10.001

Bolhar, R., Hofmann, A., Kemp, A.S., Whitehouse, M.J., Wind, S., Kamber, B.S., 2017. Juvenile crust formation in the Zimbabwe Craton deduced from the O-Hf isotopic record of 3.8-3.1 Ga detrital zircons. *Geochim. Cosmochim. Acta* **215**, 432–446. https://doi.org/10.1016/j.gca.2017.07.008

Borg, L. E., Connelly, J. N., Boyet, M., Carlson, R. W., 2011. Chronological evidence that the Moon is either young or did not have a global magma ocean. *Nature* **477**, 70-72. https://doi.org/10.1038/nature10328

Borg, L. E., Gaffney, A. M., Shearer, C. K., 2015. A review of lunar chronology revealing a preponderance of 4.34-4.37 Ga ages. *Meteorit. Planet. Sci.* **50**, 715–732. https://doi.org/10.1111/maps.12373

Borg, L. E., Gaffney, A. M., Kruijer, T. S., Marks, N. A., Sio, C. K., Wimpenny, J., 2019. Isotopic evidence for a young lunar magma ocean. *Earth Planet. Sci. Lett.* **523**, 115706. https://doi.org/10.1016/j.epsl.2019.07.008

Bouvier, A., Vervoort, J.D., Patchett, P.J., 2008. The Lu-Hf and Sm-Nd isotopic composition of CHUR: Constraints from unequilibrated chondrites and implications for the bulk composition of terrestrial planets. *Earth Planet. Sci. Lett.* **273**, 48–57. https://doi.org/10.1016/j.epsl.2008.06.010

Burkhardt, C., Kleine, T., Oberli, F., Pack, A., Bourdon, B., Wieler, R., 2011. Molybdenum isotope anomalies in meteorites: constraints on solar nebula evolution and origin of the

625 Earth. *Earth Planet. Sci. Lett.* **312**, 390–400. https://doi.org/10.1016/j.epsl.2011.10.010

626 Burton, K.W., Cenki-Tok, B., Mokadem, F., Harvey, J., Gannoun, A., Alard, O., Parkinson,
627 I.J., 2012. Unradiogenic lead in Earth's upper mantle. *Nat. Geosci.* **5**, 570–573.
628 https://doi.org/10.1038/ngeo1531

629 Canup, R.M., Asphaug, E., 2001. Origin of the Moon in a giant impact near the end of the
630 Earth's formation. *Nature* **412**, 708–712. https://doi.org/10.1038/35089010

631 Carlson, R. W., Lugmair, G.W., 1988. The age of ferroan anorthosite 60025 - Oldest crust on
632 a young moon? *Earth Planet. Sci. Lett.*, **90**, 119–130. https://doi.org/10.1016/0012-
633 821X(88)90095-7

634 Carlson, R. W., Borg, L. E., Gaffney, A. M., Boyet, M., 2014. Rb-Sr, Sm-Nd and Lu-Hf
635 isotope systematics of the lunar Mg-suite: the age of the lunar crust and its relation to
636 the time of Moon formation. *Philos. Trans. R. Soc. A Math. Phys. Eng. Sci.* **372**,
637 20130246. https://doi.org/10.1098/rsta.2013.0246

638 Chauvel, C., Goldstein, S.L., Hofmann, A.W., 1995. Hydration and dehydration of oceanic
639 crust controls Pb evolution in the mantle. *Chem. Geol.* **126**, 65–75.
640 https://doi.org/10.1016/0009-2541(95)00103-3

641 Compston, W., Kinny, P.D., Williams, I.S., Foster, J.J., 1986. The age and Pb loss behaviour
642 of zircons from the Isua supracrustal belt as determined by ion microprobe. *Earth*
643 *Planet. Sci. Lett.* **80**, 71–81. https://doi.org/10.1016/0012-821X(86)90020-8

644 Connelly, J. N., Bizzarro, M., 2016. Lead isotope evidence for a young formation age of the
645 Earth–Moon system. *Earth Planet. Sci. Lett.* **452**, 36–
646 43. https://doi.org/10.1016/j.epsl.2019.115722

647 Cumming, G.L., Richards, J.R., 1975. Ore lead isotope ratios in a continuously changing
648 earth. *Earth Planet. Sci. Lett.* **28**, 155–171. https://doi.org/10.1016/0012-
649 821X(75)90223-X

650 Davies, G.F., 1984. Geophysical and isotopic constraints on mantle convection: an interim
651 synthesis. *J. Geophys. Res.* **89**, 6017–6040. https://doi.org/10.1029/JB089iB07p06017

652 Doe, B.R., Stacey, J.S., 1974. The application of lead isotopes to the problems of ore genesis
653 and ore prospect evaluation: A review. *Econ. Geol.* **69**, 757–776.
654 https://doi.org/10.2113/gsecongeo.69.6.757

655 Frei, R., Rosing, M.T., 2001. The least radiogenic terrestrial leads; implications for the early
656 Archean crustal evolution and hydrothermal-metasomatic processes in the Isua
657 Supracrustal Belt (West Greenland). *Chem. Geol.* **181**, 47–66.
658 https://doi.org/10.1016/S0009-2541(01)00263-7

659 Gale, A., Dalton, C.A., Langmuir, C.H., Su, Y., Schilling, J.-G., 2013. The mean composition
660 of ocean ridge basalts. *Geochemistry, Geophys. Geosystems* **14**, 489–518.
661 https://doi.org/10.1029/2012GC004334

662 Galer, S.J.G., Goldstein, S.L., 1991. Depleted mantle Pb isotopic evolution using

663 conformable ore leads. In *Terra Abstr*. **3**, 485–486.

664 Galer, S.J.G., Goldstein, S.L., 1996. Influence of Accretion on Lead in the Earth. In A. Basu,
665 S.R. Hart (Eds.), Earth Processes: Reading the Isotopic Code, *Geophysical Monograph-*
666 *American Geophysical Union*, **95**, 75–98. https://doi.org/10.1029/GM095

667 Ganapathy, R., Anders, E., 1974. Bulk compositions of the moon and earth, estimated from
668 meteorites. *Lunar Planet. Sci. Conf. Proc.* **5**, 1181–1206.
669 http://adsabs.harvard.edu/full/1974LPSC....5.1181G

670 Gast, P.W., Tilton, G.R., Hedge, C., 1964. Isotopic Composition of Lead and Strontium from
671 Ascension and Gough Islands. *Science* **145**, 1181–1185.
672 https://doi.org/10.1126/science.145.3637.1181

673 Gerling, E.K., 1942. Age of the Earth according to radioactivity data. In Doklady (*Proc.*
674 *Russian Acad. Sci.*) **34**, 259–261.

675 Halliday, A. N., 2008. A young Moon-forming giant impact at 70 – 110 million years
676 accompanied by late-stage mixing, core formation and degassing of the Earth. *Philos.*
677 *Trans. R. Soc. London. Series A, Math. Phys. Sci.* **366**, 4163–4181.
678 https://doi.org/10.1098/rsta.2008.0209

679 Hart, S.R., Gaetani, G.A., 2006. Mantle Pb paradoxes: The sulfide solution. *Contrib.*
680 *Mineral. Petrol.* **152**, 295–308. https://doi.org/10.1007/s00410-006-0108-1

681 Hiess, J., Condon, D. J., McLean, N., Noble, S. R., 2012. 238U/235U systematics in
682 terrestrial uranium-bearing minerals. *Science* **335**, 1610–1614.
683 https://doi.org/10.1126/science.1215507

684 Hofmann, A.W., White, W.M., 1982. Mantle plumes from ancient oceanic crust. *Earth*
685 *Planet. Sci. Lett.* **57**, 421–436. https://doi.org/10.1016/0012-821X(82)90161-3

686 Hofmann, A.W., 2001. Lead isotopes and the age of the earth - a geochemical accident. *Geol.*
687 *Soc. London* **190**, 223–236. https://doi.org/10.1144/GSL.SP.2001.190.01.15

688 Hofmann, A.W., 2003. Sampling mantle heterogeneity through oceanic basalts: isotopes and
689 trace elements. *Treatise on Geochemistry* 61–97. https://doi.org/10.1016/B0-08-043751-
690 6/02123-X

691 Holmes, A., 1946. An Estimate of the Age of the Earth. *Nature* **157**, 680–684.
692 https://doi.org/10.1038/157336b0

693 Holzheid, A., Grove, T.L., 2002. Sulfur saturation limits in silicate melts and their
694 implications for core formation scenarios for terrestrial planets. *Am. Mineral.* **87**, 227–
695 237. https://doi.org/10.2138/am-2002-2-304

696 Houtermans, F.., 1946. Die Isotopenhäufigkeiten im natürlichen Blei und das Alter des
697 Urans. *Naturwissenschaften* **33**, 185–186. https://doi.org/10.1007/BF00585229

698 Iizuka, T., Yamaguchi, T., Hibiya, Y., Amelin, Y., 2015. Meteorite zircon constraints on the
699 bulk Lu−Hf isotope composition and early differentiation of the Earth. *Proc. Natl. Acad.*
700 *Sci.* **112**, 5331–5336. https://doi.org/10.1073/pnas.1501658112

Jaffey, A.H., Flynn, K.F., Glendenin, L.E., Bentley, W.C., Essling, A.M., 1971. Precision measurement of half-lives and specific activities of U235 and U238. *Phys. Rev. C* **4**, 1889–1906. https://doi.org/10.1103/PhysRevC.4.1889-1906

Jochum, K.P., Hofmann, A.W., Seufert, H.M., 1993. Tin in mantle-derived rocks: Constraints on Earth evolution. *Geochim. Cosmochim. Acta* **57**, 3585–3595. https://doi.org/10.1016/0016-7037(93)90141-I

Jones, J.H., Drake, M.J., 1986. Geochemical constraints on core formation in the Earth. *Nature* **322**, 221–228. https://doi.org/10.1038/322221a0

Jones, J.H., Hart, S.R., Benjamin, T.M., 1993. Experimental partitioning studies near the Fe-FeS eutectic, with an emphasis on elements important to iron meteorite chronologies (Pb, Ag, Pd, and Tl). *Geochim. Cosmochim. Acta* **57**, 453–460. https://doi.org/10.1016/0016-7037(93)90443-Z

Kamber, B.S., Collerson, K.D., 1999. Origin of ocean island basalts: A new model based on lead and helium isotope systematics. *J. Geophys. Res. Earth* **104**, 25479–25491. https://doi.org/10.1029/1999JB900258

Kiseeva, E.S., Wood, B.J., 2015. The effects of composition and temperature on chalcophile and lithophile element partitioning into magmatic sulphides. *Earth Planet. Sci. Lett.* **424**, 280–294. https://doi.org/10.1016/j.epsl.2015.05.012

Kramers, J.D., Tolstikhin, I.N., 1997. Two terrestrial lead isotope paradoxes, forward transport modelling, core formation and the history of the continental crust. *Chem. Geol.* **139**, 75–110. https://doi.org/10.1016/S0009-2541(97)00027-2

Kruijer, T. S., Kleine, T., Fischer-Gödde, M., Sprung, P., 2015. Lunar tungsten isotopic evidence for the late veneer. *Nature* **520**, 534–537. https://doi.org/10.1038/nature14360

Kruijer, T. S., Kleine, T., 2017. Tungsten isotopes and the origin of the Moon. *Earth Planet. Sci. Lett.* **475**, 15–24. http://dx.doi.org/10.1016/j.epsl.2017.07.021.

Kumari, S., Paul, D., Stracke, A., 2016. Open system models of isotopic evolution in Earth's silicate reservoirs: Implications for crustal growth and mantle heterogeneity. *Geochim. Cosmochim. Acta* **195**, 142–157. https://doi.org/10.1016/j.gca.2016.09.011

Kwon, S.T., Tilton, G.R., Grunenfelder, M.H., Bell, K., 1989. Lead isotope relationships in carbonatites and alkalic complexes: an overview. *Carbonatites Genes. Evol.* 360–387.

Laurenz, V., Rubie, D.C., Frost, D.J., Vogel, A.K., 2016. The importance of sulfur for the behavior of highly-siderophile elements during Earth's differentiation. *Geochim. Cosmochim. Acta* **194**, 123–138. https://doi.org/10.1016/j.gca.2016.08.012

Le Roux, L.A., Glendenin, L.E., 1963. Half-life of 232Th, In *Proc. Natl. Meet. Nuclear Energy*, *Pretoria, South Africa* **83**, 94.

Lee, C.-T.A., Yin, Q.-Z., Lenardic, A., Agranier, A., O'Neill, C.J., Thiagarajan, N., 2007. Trace-element composition of Fe-rich residual liquids formed by fractional crystallization: Implications for the Hadean magma ocean. *Geochim. Cosmochim. Acta* **71**, 3601–3615. https://doi.org/10.1016/j.gca.2007.04.023

Liebske, C., Corgne, A., Frost, D.J., Rubie, D.C., Wood, B.J., 2005. Compositional effects on element partitioning between Mg-silicate perovskite and silicate melts. *Contrib. Mineral. Petrol.* **149**, 113–128. https://doi.org/10.1007/s00410-004-0641-8

Liew, T.C., Milisenda, C.C., Hofmann, A.W., 1991. Isotopic contrasts, chronology of elemental transfers and high-grade metamorphism: the Sri Lanka Highland granulites, and the Lewisian (Scotland) and Nuk (SW Greenland) gneisses. *Geol. Rundschau* **80**, 279–288. https://doi.org/10.1007/BF01829366

Lodders, K., 2003. Solar System Abundances and Condensation Temperatures of the Elements. *Astrophys. J.* **591**, 1220–1247. https://doi.org/10.1086/375492

McDonough, W.F., Sun, S. s., 1995. The composition of the Earth. *Chem. Geol.* **120**, 223–253. https://doi.org/10.1016/0009-2541(94)00140-4

Moretti, R., Ottonello, G., 2005. Solubility and speciation of sulfur in silicate melts: The Conjugated Toop-Samis-Flood-Grjotheim (CTSFG) model. *Geochim. Cosmochim. Acta* **69**, 801–823. https://doi.org/10.1016/j.gca.2004.09.006

Morgan, J. W., Anders, E., 1980. Chemical composition of Earth, Venus, and Mercury. *Proc. Natl. Acad. Sci.* **77**, 6973–6977. https://doi.org/10.1073/pnas.77.12.6973

Morino, P., Caro, G., Reisberg, L., Schumacher, A., 2017. Chemical stratification in the post-magma ocean Earth inferred from coupled 146,147Sm–142,143Nd systematics in ultramafic rocks of the Saglek block (3.25–3.9 Ga; northern Labrador, Canada). *Earth Planet. Sci. Lett.* **463**, 136–150. https://doi.org/10.1016/j.epsl.2017.01.044

Murphy, D.T., Kamber, B.S., Collerson, K.D., 2003. A Refined Solution to the First Terrestrial Pb-isotope Paradox. *J. Petrol.* **44**, 39–53. https://doi.org/10.1093/petrology/44.1.39

Nemchin, A., Timms, N., Pidgeon, R., Geisler, T., Reddy, S., Meyer, C., 2009. Timing of crystallization of the lunar magma ocean constrained by the oldest zircon. *Nat. Geosci.* **2**, 133-136. https://doi.org/10.1038/ngeo417

Newsom, H.E., White, W.M., Jochum, K.P., Hofmann, A.W., 1986. Siderophile and chalcophile element abundances in oceanic basalts, Pb isotope evolution and growth of the Earth's core. *Earth Planet. Sci. Lett.* **80**, 299–313. https://doi.org/10.1016/0012-821X(86)90112-3

O'Neill, H.S.C., 1991. The origin of the Moon and the early history of the Earth - A chemical model. Part 1: The Moon. *Geochim. Cosmochim. Acta* **55**, 1135–1157. https://doi.org/10.1016/0016-7037(91)90168-5

Ostic, R.G., Russell, R.D., Stanton, R.L., 1967. Additional Measurements of the Isotopic Composition of Lead From Stratiform Deposits. *Can. J. Earth Sci.* **4**, 245–269. https://doi.org/10.1139/e67-012

Oversby, V.M., Ringwood, A.E., 1971. Time of formation of the Earth's core. *Nature* **234**, 463–465. https://doi.org/10.1038/234463a0

778 Patterson, C., 1956. Age of meteorites and the Earth. *Geochim. Cosmochim. Acta* **10**, 230–
779 237. https://doi.org/10.1016/0016-7037(56)90036-9

780 Peucker-Ehrenbrink, B., Hofmann, A.W., Hart, S.R., 1994. Hydrothermal lead transfer from
781 mantle to continental crust: the role of metalliferous sediments. *Earth Planet. Sci. Lett.*
782 **125**, 129–142. https://doi.org/10.1016/0012-821X(94)90211-9

783 Render, J., Fischer-Gödde, M., Burkhardt, C., Kleine, T., 2017. The cosmic molybdenum-
784 neodymium isotope correlation and the building material of the Earth. *Geochemical*
785 *Perspect. Lett.* 170–178. https://doi.org/10.7185/geochemlet.1720

786 Richards, J. R., 1971. Major Lead Orebodies--Mantle Origin? *Econ. Geol.* **66**, 425–434.
787 https://doi.org/10.2113/gsecongeo.66.3.425

788 Richards, J.R., 1977. Lead isotopes and ages of Galenas from the Pilbara region, Western
789 Australia. *J. Geol. Soc. Aust.* **24**, 465–473. https://doi.org/10.1080/00167617708729006

790 Richards, J.R., Fletcher, I.R., Blockley, J.G., 1981. Pilbara galenas: Precise isotopic assay of
791 the oldest Australian leads; model ages and growth-curve implications. *Miner. Depos.*
792 **16**, 7–30. https://doi.org/10.1007/BF00206451

793 Righter, K., 2011. Prediction of metal-silicate partition coefficients for siderophile elements:
794 An update and assessment of PT conditions for metal-silicate equilibrium during
795 accretion of the Earth. *Earth Planet. Sci. Lett.* **304**, 158–167.
796 https://doi.org/10.1016/j.epsl.2011.01.028

797 Rubie, D.C., Jacobson, S.A., Morbidelli, A., O'Brien, D.P., Young, E.D., de Vries, J.,
798 Nimmo, F., Palme, H., Frost, D.J., 2015. Accretion and differentiation of the terrestrial
799 planets with implications for the compositions of early-formed Solar System bodies and
800 accretion of water. *Icarus* **248**, 89–108. https://doi.org/10.1016/j.icarus.2014.10.015

801 Russell, R. D., 1956. Lead isotopes as a key to the radioactivity of the Earth's mantle. *Ann. N.*
802 *Y. Acad. Sci.* **62**, 437–448. https://doi.org/10.1111/j.1749-6632.1956.tb35362.

803 Saager, R., Köppel, V., 1976. Lead Isotopes and Trace Elements from Sulfides of Archcan
804 Greenstone Belts in South Africa Knowledge of the Oldest Known Mineralizations of
805 sulfides deposits in the Swaziland. *Geology* **71**, 44–57.
806 https://doi.org/10.2113/gsecongeo.71.1.44

807 Sinha, A.K., 1972. U-Th-Pb systematics and the age of the Onverwacht Series, South Africa.
808 *Earth Planet. Sci. Lett.* **16**, 219–227. https://doi.org/10.1016/0012-821X(72)90193-8

809 Snape, J. F., Nemchin, A. A., Bellucci, J. J., Whitehouse, M. J., Tartèse, R., Barnes, J. J.,
810 Anand, M., Crawford, I. A., Joy, K. H., 2016. Lunar basalt chronology, mantle
811 differentiation and implications for determining the age of the Moon. *Earth Planet. Sci.*
812 *Lett.* **451**, 149–158. http://dx.doi.org/10.1016/j.epsl.2016.07.026.

813 Stacey, J.S., Kramers, J., 1975. Approximation of terrestrial lead isotope evolution by a two-
814 stage model. *Earth Planet. Sci. Lett.* **26**, 207–221. https://doi.org/10.1016/0012-
815 821X(75)90088-6

816 Stanton, R. L., Russell, R. D., 1959. Anomalous leads and the emplacement of lead sulfide

817 ores. *Economic Geology*, **54(4)**, 588-607. https://doi.org/10.2113/gsecongeo.54.4.588

818 Staudigel, H., Davies, G.R., Hart, S.R., Marchant, K.M., Smith, B.M., 1995. Large scale
819 isotopic Sr, Nd and O isotopic anatomy of altered oceanic crust: DSDP/ODP
820 sites417/418. *Earth Planet. Sci. Lett.* **130**, 169–185. https://doi.org/10.1016/0012-
821 821X(94)00263-X

822 Sun, S.-S., 1982. Chemical composition and origin of the Earth's primitive mantle. *Geochim.*
823 *Cosmochim. Acta* **46**, 179–192. https://doi.org/10.1016/0016-7037(82)90245-9

824 Tatsumoto, M., Knight, R.J., Allègre, C.J., 1973. Time differences in the formation of
825 meteorites as determined from the ratio of lead-207 to lead-206. *Science (80-.).* **180**,
826 1279–1283. https://doi.org/10.1126/science.180.4092.1279

827 Thiemens, M. M., Sprung, P., Fonseca, R. O. C., Leitzke, F. P., Münker, C., 2019. Early
828 Moon formation inferred from hafnium–tungsten systematics. *Nat. Geosci.* **12**, 696–700.
829 http://dx.doi.org/10.1038/s41561-019-0398-3.

830 Thorpe, R.I., Hickman, A.H., Davis, D.W., Mortensen, J.K., Trendall, A.F., 1992. U-Pb
831 zircon geochronology of Archaean felsic units in the Marble Bar region, Pilbara Craton,
832 Western Australia. *Precambrian Res.* **56**, 169–189. https://doi.org/10.1016/0301-
833 9268(92)90100-3

834 Tilton, G.R., Barreiro, B.A., 1980. Origin of Lead in Andean Calc-Alkaline Lavas, Southern
835 Peru. *Science (80-.).* **210**, 1245–1247. https://doi.org/10.1126/science.210.4475.1245

836 Touboul, M., Puchtel, I.S., Walker, R.J., 2015. Tungsten isotopic evidence for
837 disproportional late accretion to the Earth and Moon. *Nature* **520**, 530–533.
838 https://doi.org/10.1038/nature14355

839 Ulrych, T.J., Burger, A., Nicolaysen, L.O., 1967. Least radiogenic terrestrial leads. *Earth*
840 *Planet. Sci. Lett.* **2**, 179–184. https://doi.org/10.1016/0012-821X(67)90125-2

841 Wade, J., Wood, B.J., 2005. Core formation and the oxidation state of the Earth. *Earth*
842 *Planet. Sci. Lett.* **236**, 78–95. https://doi.org/10.1016/j.epsl.2005.05.017

843 Wang, Z., Becker, H., 2013. Ratios of S, Se and Te in the silicate Earth require a volatile-rich
844 late veneer. *Nature* **499**, 328–331. https://doi.org/10.1038/nature12285

845 Wang, H.S., Lineweaver, C.H., Ireland, T.R., 2018. The elemental abundances (with
846 uncertainties) of the most Earth-like planet. *Icarus* **299**, 460–474.
847 https://doi.org/10.1016/j.icarus.2017.08.024

848 Wänke, H., 1981. Constitution of terrestrial planets. *Philos. Trans. R. Soc. London. Ser. A,*
849 *Math. Phys. Sci.* **303**, 287–302. https://doi.org/10.1098/rsta.1981.0203

850 Wänke, H., Dreibus, G., 1988. Chemical composition and accretion history of terrestrial
851 planets. *Philos. Trans. R. Soc. London. Ser. A, Math. Phys. Sci.* **325**, 545–557.
852 https://doi.org/10.1098/rsta.1988.0067

853 Wilde, S. A., Valley, J. W., Peck, W. H., Graham, C. M., 2001. Evidence from detrital
854 zircons for the existence of continental crust and oceans on the Earth 4.4 Gyr ago.

Nature **409**, 175–178. https://doi.org/10.1038/35051550

Wilson, J. T., Russell, R. D., Farquhar, R. M., 1956. Radioactivity and age of minerals. *Geophys. I/Geophysics I*, 288–363. https://doi.org/10.1007/978-3-642-45855-2_11

Wipperfurth, S.A., Guo, M., Šrámek, O., McDonough, W.F., 2018. Earth's chondritic Th/U: Negligible fractionation during accretion, core formation, and crust–mantle differentiation. *Earth Planet. Sci. Lett.* **498**, 196–202. https://doi.org/10.1016/j.epsl.2018.06.029

Wohlers, A., Wood, B.J., 2017. Uranium, thorium and REE partitioning into sulfide liquids: Implications for reduced S-rich bodies. *Geochim. Cosmochim. Acta* **205**, 226–244. https://doi.org/10.1016/j.gca.2017.01.050

Wood, B.J., Halliday, A.N., 2005. Cooling of the Earth and core formation after the giant impact. *Nature* **437**, 1345–1348. https://doi.org/10.1038/nature04129

Wood, B.J., Walter, M.J., Wade, J., 2006. Accretion of the Earth and segregation of its core. *Nature* **441**, 825–833. https://doi.org/10.1038/nature04763

Zartman, R.E., Doe, B.R., 1981. Plumbotectonics - the model. *Tectonophysics* **75**, 135–162. https://doi.org/10.1016/0040-1951(81)90213-4

Zartman, R.E., Haines, S.M., 1988. The plumbotectonic model for Pb isotopic systematics among major terrestrial reservoirs-A case for bi-directional transport. *Geochim. Cosmochim. Acta* **52**, 1327–1339. https://doi.org/10.1016/0016-7037(88)90204-9

Zindler, A., Hart, S., 1986. Chemical Geodynamics. *Annu. Rev. Earth Planet. Sci.* **14**, 493–571. https://doi.org/10.1146/annurev.ea.14.050186.002425

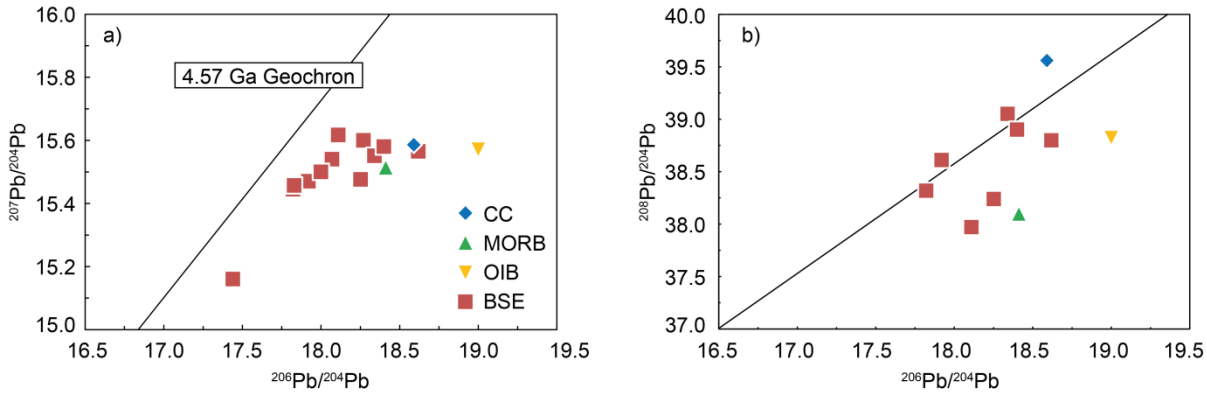

Fig. 1: Illustration of the 1st Pb paradox. (a) Estimated $^{207}Pb/^{204}Pb$ vs $^{206}Pb/^{204}Pb$ of BSE. All average isotope compositions of the displayed terrestrial reservoirs plot to the right of the 4.57 Ga Geochron. Consequently, this is also the case for all estimates of the BSE. By

definition the Pb isotope composition of BSE has to plot on the true Geochron, since BSE is a theoretical reservoir that remained a closed system after core formation. (b) Estimated $^{208}Pb/^{204}Pb$ vs $^{206}Pb/^{204}Pb$ of BSE. Isotope ratios for CC from Allègre & Lewin (1989), MORB from Gale et al. (2013), and OIB from Kumari et al. (2016). BSE literature estimates as displayed in Fig. 4.

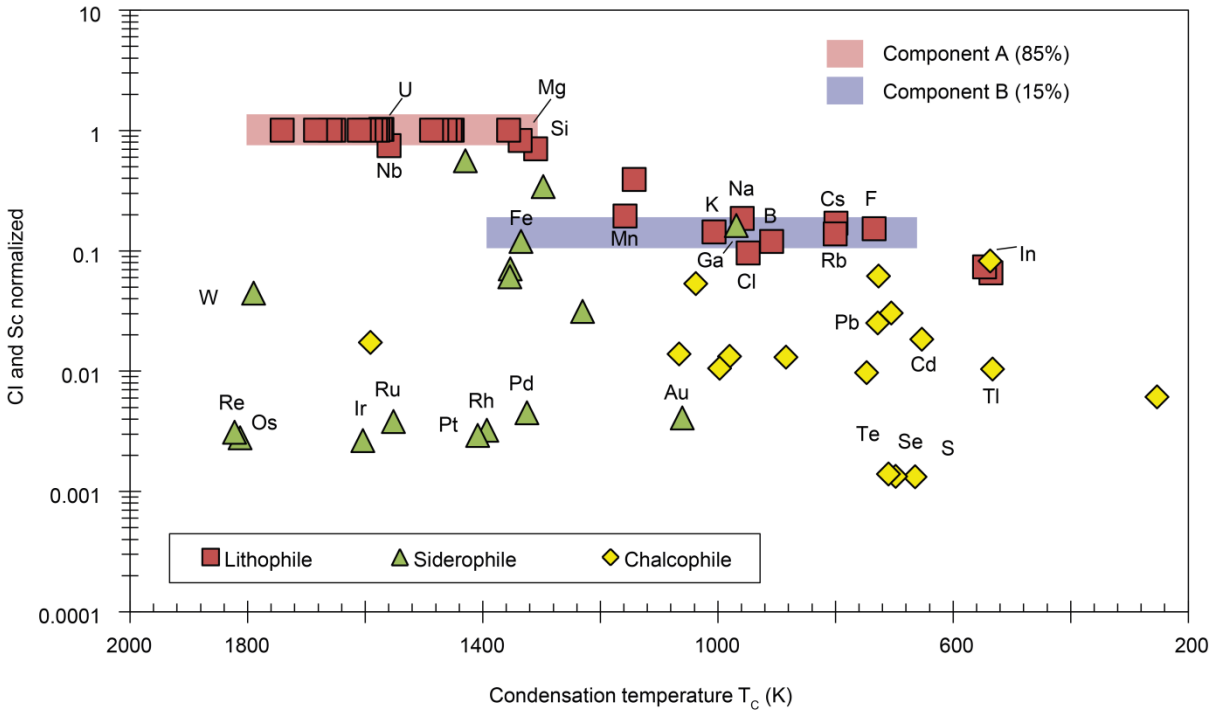

Fig. 2: Estimates of element abundances in BSE normalized to CI carbonaceous chondrites and Sc against their condensation temperature in the solar nebula (50 % T_C). The relative abundances of the lithophile elements can be approximated by a step function, representative of two component mixing, rather than following a poorly defined depletion trend as a function of condensation temperature. Element abundances from McDonough & Sun (1995), Lodders (2003), and Wang et al. (2018).

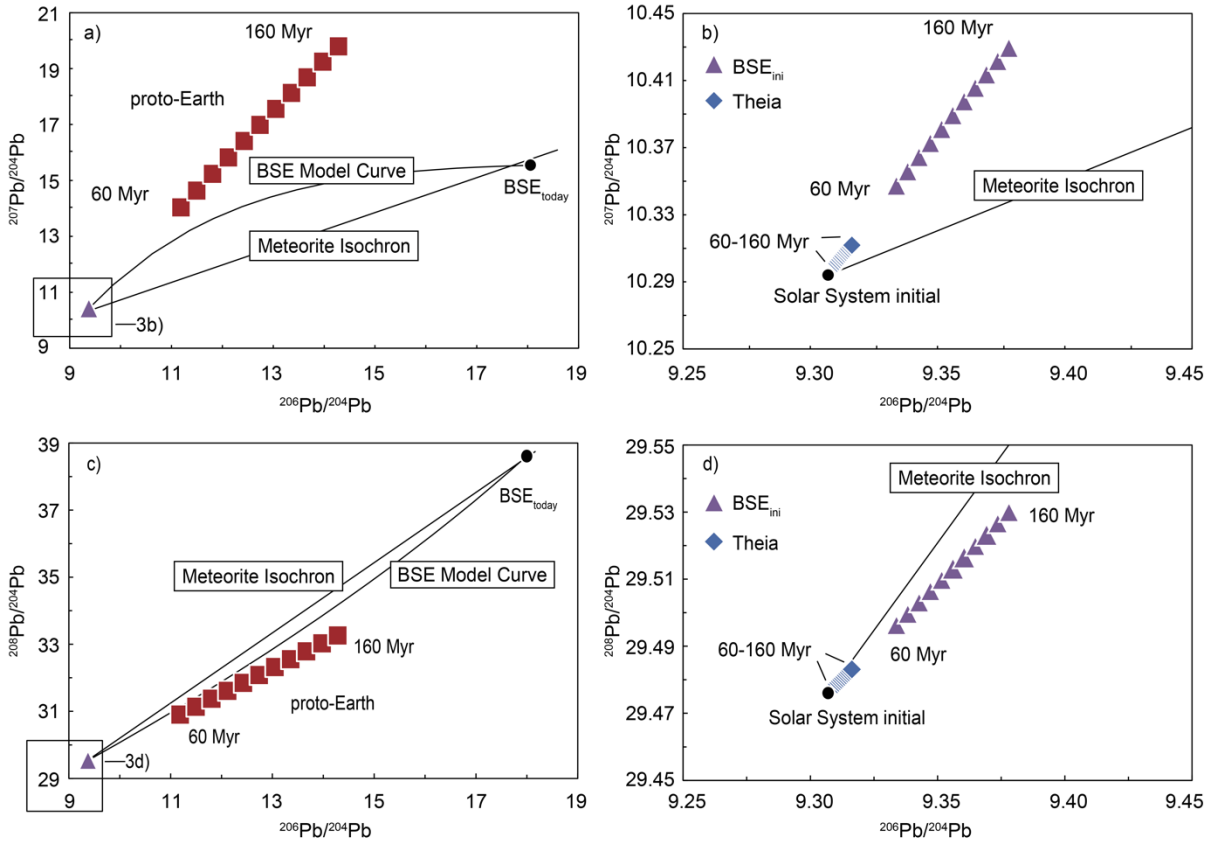

Fig. 3: (a) and (b): Illustration of the mixing model in $^{207}Pb/^{204}Pb$ vs $^{206}Pb/^{204}Pb$ isotope space for BSE. Theia (blue diamonds) and silicate portion of proto-Earth (red squares) evolved independently from the Canyon Diablo solar system initial before being mixed in proportions of 15 and 85 %. Isotope compositions are shown from 60 to 160 Myr after the formation of the solar system, in steps of 10 Myr. Proto-Earth evolved rapidly to high isotope ratios due to the low abundance of ^{204}Pb. In contrast, Pb in Theia did not evolve much beyond its initial composition, due to its similarity to CI chondrites. The BSE mixing array (purple triangles, BSE_{ini}) plots much closer to Theia, due to the strong depletion in volatile elements (including Pb) in proto Earth. (c) and (d): equivalent to (a) and (b) for $^{208}Pb/^{204}Pb$ vs $^{206}Pb/^{204}Pb$ isotope space.

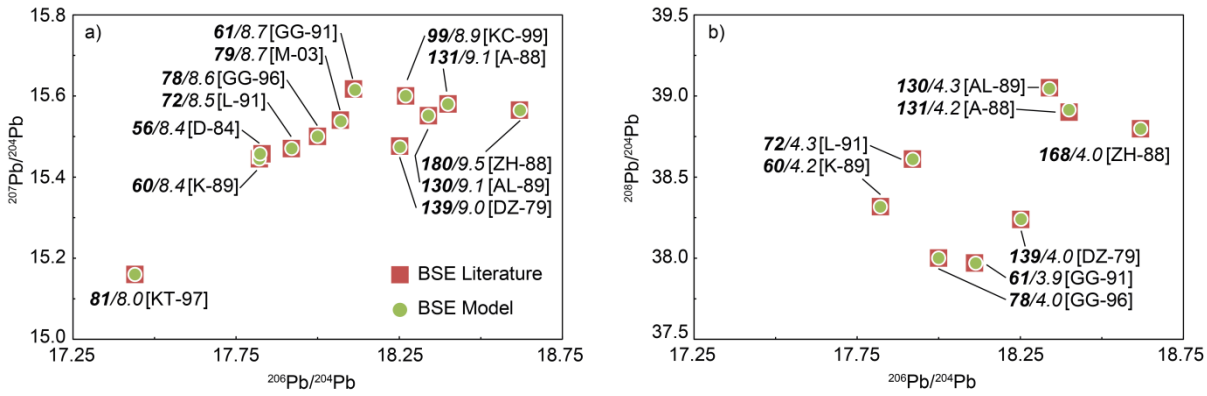

908

909 Fig. 4: Results from the model calculations for each BSE literature estimate. (a) Bold
910 characters indicate the time the model composition intersects with the BSE_{ini} mixing array,
911 followed by the required μ-value. Each literature estimate can only be solved for one specific
912 point in time. (b) Equivalent to (a) but with κ instead of μ. Fewer values are shown because
913 not all studies provide estimates for $^{208}Pb/^{204}Pb$. BSE estimates from [DZ-79] Doe & Zartman
914 (1979); [D-84] Davies (1984); [A-88] Allègre et al. (1988); [ZH-88] Zartman & Haines
915 (1988); [AL-89] Allègre & Lewin (1989); [K-89] Kwon et al. (1989); [L-91] Liew et al.
916 (1991); [GG-91]/[GG-96] Galer & Goldstein (1991, 1996); [KT-97] Kramers & Tolstikhin
917 (1997); [KC-99] Kamber & Collerson (1999); [M-03] Murphy et al. (2003).

918

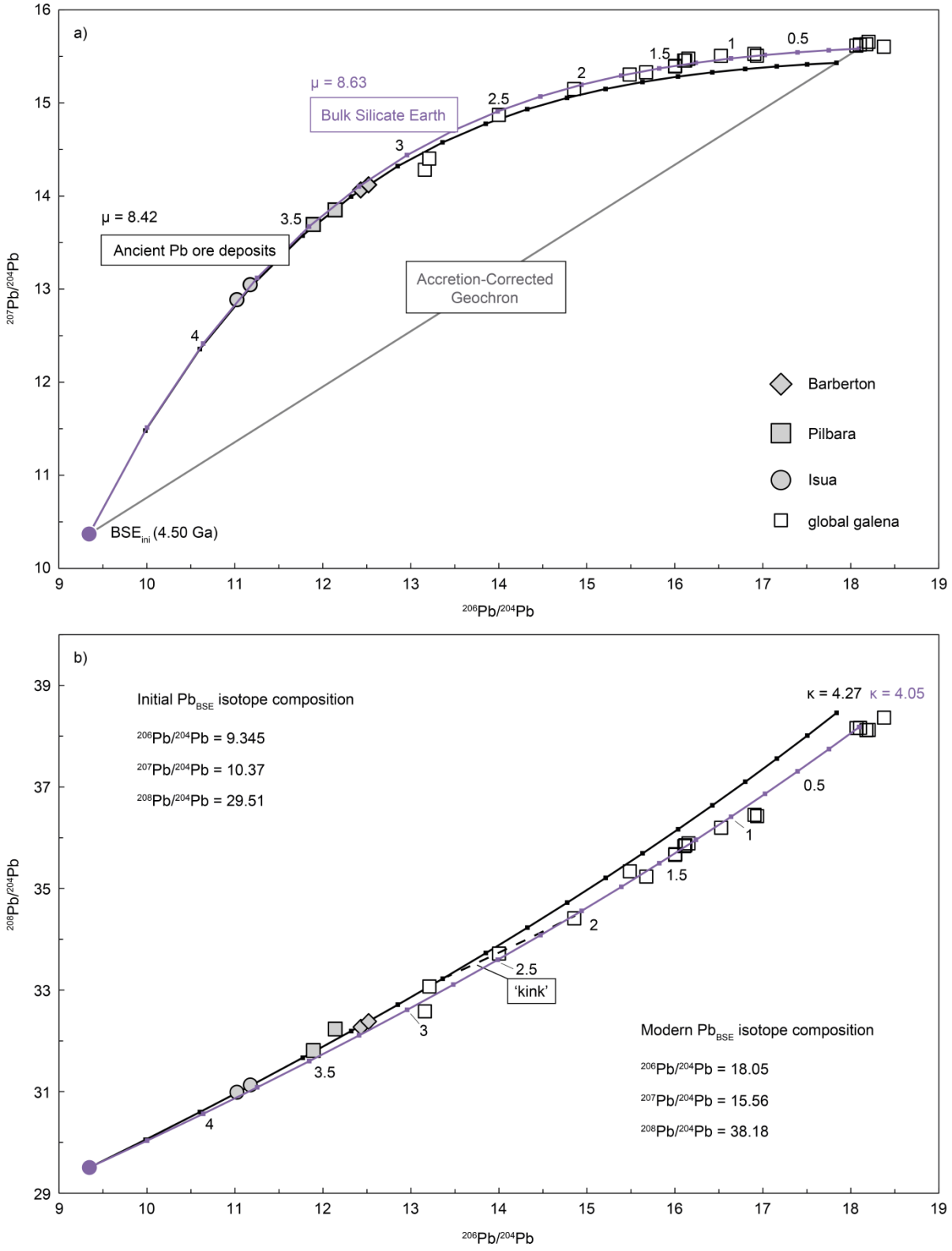

Fig. 5: Comparison of Pb isotope evolution curves in ^{208}Pb-^{207}Pb vs. ^{206}Pb-^{204}Pb isotope space. The initial BSE isotope composition is calculated for 69 Myr after beginning of the

923 solar system, as derived from the cluster of younger ages in Fig. 4. The same cluster is used
924 for μ_{BSE} and κ_{BSE} allowing construction of the bulk silicate Earth model (purple curve). Grey
925 symbols are used to fit the black curve using a least squares linear regression, as well as for
926 model age calculations displayed in Table 3. Open symbols are not included in calculations
927 and represent data from other globally available stratiform deposits, pooled from Stacey &
928 Kramers (1975) and Cumming & Richards (1975). The 'kink' in (b) refers to the observed
929 gradual change in κ-value from the ancient galena ($\kappa = 4.27$) source back towards the modern
930 mass weighted best estimate of $\kappa_{BSE} = 3.90$ (Wipperfurth et al., 2018).
931

Table 1: Parameters BSE_{ini} mixing model

	Component A proto-Earth	Component B Theia
relative size (%)	85.2 (9)[1]	14.8 (9)[1]
^{238}U (mol/g)	5.00×10^{-11}	3.38×10^{-11}
^{204}Pb (mol/g)	5.00×10^{-13}	1.80×10^{-10}
μ	100	0.188
κ	3.90	3.90
$^{206}Pb/^{204}Pb_{ini}$	9.307	9.307
$^{207}Pb/^{204}Pb_{ini}$	10.294	10.294
$^{208}Pb/^{204}Pb_{ini}$	29.476	29.476

[1] error in the last significant digit, from S-Table 1

Table 2: BSE_{ini} mixing ages (t_{mix})

	t_{mix}[1]	±	μ	± (%)	ω	± (%)	κ	± (%)
D-84	56	2	8.38	0.06				
K-89	60	2	8.38	0.08	35.3	0.03	4.21	0.06
GG-91	61	1	8.67	0.01	33.9	0.00	3.91	0.08
L-91	72	2	8.50	0.09	36.6	0.00	4.30	0.09
GG-96	78	1	8.59	0.01	34.3	0.00	3.99	0.03
M-03	79	2	8.67	0.06				
KT-97	81	2	8.05	0.00				
KC-99	99	2	8.91	0.03				
AL-89	130	3	9.05	0.07	38.8	0.05	4.28	0.04
A-88	131	3	9.11	0.02	38.2	0.03	4.19	0.05
DZ-79	139	3	8.98	0.03	35.5	0.00	3.96	0.07
ZH-88	180	4	9.45	0.03	38.1	0.00	4.04	0.02
Wtd. avg. 1*	69	10	8.63	0.74	34.8	6.0	4.05	5.4
Wtd. avg. 2	125	34	9.12	2.6	36.7	6.5	4.08	4.4

[1] time of mixing of component A and B in Myr after the start of the solar system

*Wtd. avg. 1 = D-84 to MKC-03, Wtd. avg. 2 = KC-99 to ZH-88, with 95 % conf. absolute errors

Table 3: Comparison of most primitive Pb isotope signatures of galena from ancient ore deposits and BSE isotope compositions for the same age

	$^{206}Pb/^{204}Pb$			$^{207}Pb/^{204}Pb$			$^{208}Pb/^{204}Pb$			geological	model
sample	literature	model	% delta	literature	model	% delta	literature	model	% delta	age [Ga]	age [Ga][f]
					Isua, Greenland[1]						
460000-1	11.02	11.11	0.77	12.89	12.96	0.58	30.99	30.97	0.07	3.807[a]	3.862
Pb539	11.18	11.27	0.80	13.05	13.13	0.63	31.13	31.10	0.09	3.741[b]	3.791
					Pilbara, Western Australia[2,3]						
Big Stubby	11.89	11.90	0.06	13.69	13.71	0.14	31.81	31.66	0.47	3.471[c]	3.462
Doolena Gap	12.14	12.22	0.66	13.85	13.96	0.79	32.23	31.95	0.88	3.329[c]	3.320
					South Africa[4,5]						
Daylight	12.43	12.51	0.61	14.07	14.16	0.66	32.27	32.21	0.19	3.200[d]	3.198
Rosetta	12.52	12.60	0.60	14.12	14.22	0.67	32.38	32.29	0.28	3.160[e]	3.154

References: 1, Frei & Rosing, 2001; 2, Richards et al., 1981; 3, Richards, 1977; 4, Ulrych et al., 1967; 5, Saager & Köppel, 1976

[a] U-Pb zircon age, Baadsgaard et al., 1984; Compston et al., 1986

[b] tourmaline-bulk sphalerite isochron, Frei & Rosing, 2001

[c] Thorpe et al., 1992

[d] max. stratigraphic age, Cumming & Richards, 1975

[e] Pb-Pb, U-Pb whole rock; min. age for Onverwacht group, Sinha, 1972

[f] $^{207}Pb/^{206}Pb$ model isochron age derived from BSE_{ini} and galena isotope compositions

Supplementary Material

S-Table 1: Size estimate component B

Element	Cl and Sc normalized
F	0.152
Cs	0.170
Rb	0.137
B	0.119
Cl	0.096
Na	0.185
Ga	0.162
K	0.143
Mn	0.194
Fe	0.120
Avg.	0.148
S. d.[1]	0.009

[1] standard deviation of the mean

S-Table 2: BSE model curve

t_{mix} [1]	μ	ω	κ
69	8.63	34.8	4.05
t [Ga]	$^{206}Pb/^{204}Pb$	$^{207}Pb/^{204}Pb$	$^{208}Pb/^{204}Pb$
4.50	9.345	10.37	29.51
4.25	10.00	11.51	30.04
4.00	10.63	12.41	30.56
3.75	11.24	13.11	31.08
3.50	11.83	13.66	31.60
3.25	12.40	14.09	32.11
3.00	12.94	14.42	32.61
2.75	13.46	14.68	33.11
2.50	13.97	14.89	33.60
2.25	14.45	15.05	34.08
2.00	14.92	15.17	34.56
1.75	15.36	15.27	35.03
1.50	15.79	15.35	35.50
1.25	16.21	15.41	35.96
1.00	16.61	15.45	36.41
0.75	16.99	15.49	36.86
0.50	17.36	15.52	37.31
0.25	17.71	15.54	37.75
0.00	18.05	15.56	38.18

[1] time of mixing of component A and B in Myr after the start of the solar system